Radar-based Fall Detection Based on Doppler Time-Frequency Signatures for Assisted Living

Qisong Wu, Yimin D. Zhang, Wenbing Tao, and Moeness G. Amin

Abstract

Falls are a major public health concern and main causes of accidental death in the senior U.S. population. Timely and accurate detection permits immediate assistance after a fall and, thereby, reduces complications of fall risk. Radar technology provides an effective means for this purpose because it is non-invasive, insensitive to lighting conditions as well as obstructions, and has less privacy concerns. In this paper, we develop an effective fall detection scheme for the application in continuous-wave radar systems. The proposed scheme exploits time-frequency characteristics of the radar Doppler signatures, and the motion events are classified using the joint statistics of three different features, including the extreme frequency, extreme frequency ratio, and the length of event period. Sparse Bayesian classifier based on the relevance vector machine is used to perform the classification. Laboratory experiments are performed to collect radar data corresponding to different motion patterns to verify the effectiveness of the proposed algorithm.

Index Terms

Assisted living, fall detection, time-frequency analysis, sparse Bayesian classification, relevance vector machine.

This paper is made possible by NPRP Grant # NPRP 6-680-2-282 from the Qatar National Research Fund (a member of Qatar Foundation). The statements made herein are solely the responsibility of the authors. Part of the results has been presented at the SPIE Radar Sensor Technology XVIII Conference, Baltimore, MD, May 2014 [1] and the IEEE China Summit and International Conference on Signal and Information Processing, Xi'an, China, July 2014 [2].

Q. Wu, Y. D. Zhang, and M. G. Amin are with the Center for Advanced Communications, Villanova University, Villanova, PA 19085, USA.

W. Tao is with the School of Automation, Huazhong University of Science and Technology, Wuhan 430074, China.

I. Introduction

The old-age dependency ratio, which is defined as the ratio of the population aged 65-years or over to the population aged between 20 and 64 and represents the number of dependents per 100 persons of working age, has been rising in many countries all over the world. According to United Nations estimates for the "more developed regions", this ratio is anticipated to exceed 30% in 2020 and reach 40% in 2030 [3]. To address the challenges of self-dependence living within homes or residences for the elderly population, therefore, assisted living is an emerging area that involve a broad spectrum of scientists. Among these challenges, elderly falls are a major public health concern as they often result in disability and the main cause of accidental death in the U.S. population over age 65 [4], [5]. Because immediate assistance provided after a fall can significantly reduce complications of fall risks, it is critical to detect elderly falls in a timely and accurate manner so that immediate response and proper care can be rendered [6].

Recent advances in sensing technologies can help reduce injuries and provide early detection of health declination. This, in turn, leads to timely interventions and most effective treatments. Sensing apparatuses depend on active and continuous assessments of health conditions and motor functional abilities of the elderly so that small changes from predefined baseline can be detected. A number of techniques have been proposed to sense vital signs and motions for ambient assisted living (see, for example, [7], [8], [9]). These sensing techniques include those monitoring physiological signs (e.g., electrocardiography (ECG)) and accelerometers, video camera, passive infrared and thermography sensors, laser vibrometer, and radio frequency identification (RFID) devices. Among those, ECG, accelerometers, and RFID require that devices be attached to human body, whereas laser vibrometer requires very accurate control or placement. On the other hand, video camera systems are sensitive to lighting conditions and obstructions due to walls and fabrics, and raise privacy concerns.

Radar is an excellent sensing modality for elderly fall detection due to its capability of monitoring human motions. The general concept of radar-based system is to transmit an electromagnetic (EM) wave over a certain range of frequencies and analyze the radar return signals. Radar systems offer non-intrusive, clutter suppressed and noise tolerant sensing systems for sensing moving human objects [10]. Specifically, low-cost narrowband radar systems can be used to estimate the instantaneous velocity of moving objects by measuring the frequency shift of the wave beckscattered from the object, known as the Doppler effects [11]. For an articulated object such as a walking person, the motion of various components of the body, including the torso, arms, and legs, induces frequency modulations on the returned radar signal, referred to as Doppler signatures. As such, they enable monitoring of the elderlies motion profiles in their private homes as well as in healthcare facilities. Radar systems avoid direct contact (unlike ECG and accelerometers) and do not require very accurate control or placement (unlike laser Doppler vibrometer). Compared to optical and infrared (IR)-based systems, radar systems can operate in all types of environments, can penetrate walls and fabrics, preserve privacy, and are insensitive to lighting conditions.

The human gait classification based on radar Doppler spectrograms was considered for different arm motion patterns in the context of urban sensing [12], [13], [14], [15], [16]. In [14], [15], [16], a common scheme applied in these algorithms is to extract the Doppler signature features, based on which the motion patterns are then identified using the support vector machine (SVM). SVM is a state-of-the-art learning system that is commonly used in practice for pattern recognition and data mining applications, such as text categorization, image classification, and bioinformatics [17], [18]. However, SVM is known to make unnecessarily liberal use of basis functions since the number of required support vectors typically grows linearly with the size of the training set and, therefore, is not preferred in processing large-scale data sets. In addition, it requires that the error/margin trade-off parameters to be validated. The kernel matching pursuit (KMP) [19], which greedily selects basis functions for non-regularized kernel least squares problem, was proposed to achieve comparable accuracy by utilizing reduced number of support vectors in the classifier. The SVM with reduced classifier complexity [20] extended the basic ideas of KMP to the SVM. Nevertheless, ‘nuisance’ parameters, such as the number of support vectors [19], trade-off parameters [20], and input variable scales in the kernel function [19], [20], are still required to validate these approaches. In addition, the predictions of these approaches are not probabilistic and their outputs are hard binary decisions.

In this paper, we examine a different approach for radar-based fall detection based on the time-frequency characteristics of the radar return. Potentially catastrophic events are first identified by applying the short-time Fourier transform (STFT) to the raw data retrieved from the radar and analyzing the energy content of the signal. These events are extracted from the data for a tri-characteristic analysis in order to classify the type of motion. The sparse Bayesian classification algorithm is examined to distinguish between different motion patterns that respectively exhibit close and distinct Doppler signatures. It has been demonstrated that sparse Bayesian learning methods based on the relevance vector machine (RVM) [21], [22] improve performances over the SVM with fewer relevance vectors. RVM is also a discriminative modeling technique in a form similar to the SVM, but it is a fully probabilistic model and enables to estimate the conditional probability distribution in order to capture the uncertainty in the prediction, unlike the hard point estimation in the SVM. Furthermore, there are no parameters to validate in the sense that the maximum likelihood procedure automatically sets the ‘regularisation’ parameters

[21].

The proposed technique is tested using experimental data collected at the Radar Imaging Lab, Center for Advanced Communications, Villanova University. For fall detection purpose, we have designed fall events including forward and backward falls, and non-fall events including sitting-and-standing (S&S) motions, and bending over and standing up (B&S) motions for classification. With the data collected, we obtained quantifiable results to verify the reliability of the proposed classification algorithm.

This paper is organized as follows. The system and signal models are described in Section II. The Sparse Bayesian classification technique is introduced in Section III. We then describe the proposed feature and classification techniques in Section IV. Section V provides the processed results of the experimental data, Section VI concludes this paper.

The following notations are used in this paper. A lower (upper) case bold letter denotes a vector (matrix). $(.)^T$ denotes transpose, and $\|\cdot\|$ represents the l_2 norm of a vector. Furthermore, $\mathcal{N}(a,b)$ denotes normal distribution with mean a and variance b, $\mathrm{diag}(.)$ converts a vector or a row sequence into a diagonal matrix, and $|\mathbf{A}|$ denotes the determinant of matrix $\mathbf{A}$.

II. System and Signal Model

A. Signal Model

Consider a continuous-wave (CW) radar which emits a sinusoidal signal with frequency f_c over the sensing period. The transmitted waveform is expressed as $s(t) = \exp(j2\pi f_c t)$. Let us first consider a point target which is located at a distance of R_0 from the radar at time instant t_0, and moves with a velocity of $v(t)$ toward a direction which forms an angle of θ between the radar direction. As such, the distance between the radar and the target at time instant t is expressed as

$$R(t) = R_0 + \int_{t_0}^{t} v(u)\cos(\theta)du, \tag{1}$$

and the received radar signal is expressed as

$$x_a(t) = \rho \exp[j2\pi f_c(t - 2R(t)/c)], \tag{2}$$

where ρ is the target reflection coefficient and c is the velocity of EM wave propagation. The Doppler frequency corresponding to $x_a(t)$ is

$$f_D(t) = 2v(t)\cos(\theta)/\lambda, \tag{3}$$

where $\lambda = c/f_c$ is the wavelength.

A rigid body target, such as a human body, can be considered as a collection of scatterers. Therefore, the return signal is the integration over the target region, expressed as

$$x(t) = \int_{\Omega} x_a(t)da, \tag{4}$$

where Ω denotes the target region. As such, the Doppler signature is the superposition of each component Doppler frequencies. Torso or gait motions generally generate different time-varying Doppler frequencies, and their exact signatures depend on the target shape and the motion patterns.

In our experimental studies, the radar data sets were collected in the Radar Imaging Lab at the Center for Advanced Communications, Villanova University. The experiment scene is shown in Fig. 1. The laboratory is semi-controlled by placing EM absorbers around the walls to reduce the effect of wall reflection. An Agilent network analyzer was externally triggered with a time sampling rate of 1 kHz, and the carrier frequency is $f_c = 8$ GHz. The network analyzer records backscattering coefficients in terms of magnitude and phase, and the results are converted into complex expressions, $x_r(t)$. In addition, background signals $x_0(t)$ in the absence of target are also collected and their effect are subtracted from all data observations. As such, the data to be processed for Doppler analysis is expressed as

$$x(t) = x_r(t) - x_0(t), \tag{5}$$

which is periodically sampled to result in discrete-time observations $x[k] = x(kT)$, where $T = 10^{-3}$ s is the sampling interval.

Fig. 1. Experiment scene.

B. Time-Frequency Analysis

By using joint time-frequency analysis methods, time-varying Doppler frequency can be captured at various instances of time. In this paper, we use the spectrogram, generated through the STFT, to perform the time-frequency analysis of the Doppler signature. The discrete-time

STFT of signal $x(t)$ is defined as

$$X[k,\nu] = \sum_{m=-\infty}^{\infty} x[m]h[k-m]\exp(-j2\pi m\nu TF), \tag{6}$$

where ν denotes the index of frequency bin (νF is the actual frequency with F denoting the frequency step size), and $h[k]$ is the discrete-time window function that trades off the time and frequency resolutions. We use the Hamming window and tested different window sizes and found that a window size of 255 is chosen for our processing. A larger window length may degrade the time resolution whereas as a smaller window length may compromise the frequency resolution. Fig. 2 compares the spectrogram, which is the magnitude square of the STFT, of a backward fall with Hamming window sizes of 127, 255, 511, and 1023.

C. Power Burst Curve

After the proper spectrogram of the data is obtained, the algorithm first determines exactly where important events have occurred in the data and a classification process should be initiated to detect whether such an event is a fall. We utilize a power burst curve (PBC) of the data (which was referred to as the energy burst curve in [23] and [24]), which represents the summation of signal power within a specific frequency band between frequencies f_1 and f_2 at time instant kT, expressed as

$$PBC[k] = \sum_{\nu:\nu F\in[f_1,f_2]} |X[k,\nu]|^2 + \sum_{\nu:\nu F\in[-f_2,-f_1]} |X[k,\nu]|^2. \tag{7}$$

We choose $f_1 = 70$ Hz and $f_2 = 100$ Hz to detect high-energy events, as catastrophic events, such as falls, typically have high Doppler energy content within this frequency band.

The PBC of the ambient noise can be considered to follow a Gaussian distribution, denoted as $\mathcal{N}(\mu_P, \sigma_P)$, where μ_P and σ_P respectively denote the mean and variance of the distribution.

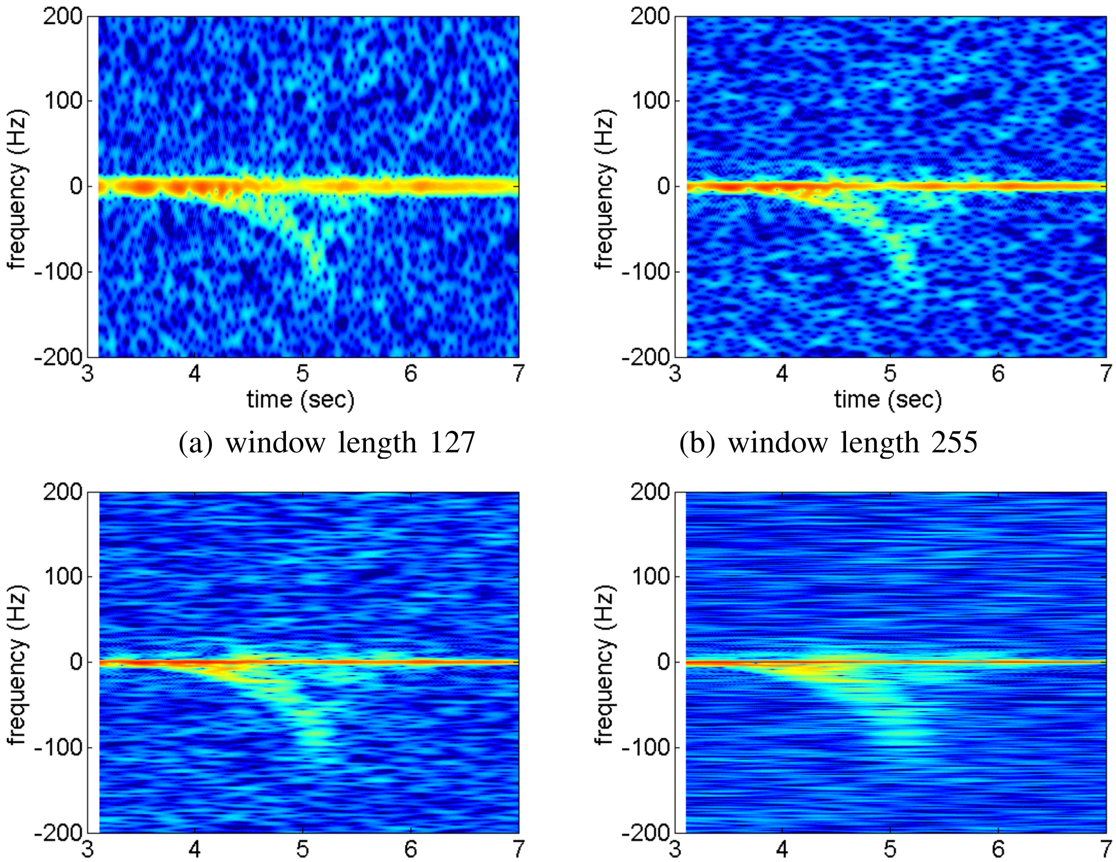

(a) window length 127 (b) window length 255

(c) window length 511 (d) window length 1023

Fig. 2. Spectrogram of fall generated with different window sizes.

To keep the algorithm sensitive to human event whereas sufficiently separated from the noise power burst floor, the following threshold is used for event detection:

$$\eta_P = \mu_P + 6\sqrt{\sigma_P}. \tag{8}$$

Therefore, an event is determined whenever the PBC exceeds threshold η_P, initiating the classification procedure as described in the following section. Fig. 3 shows one example of the PBC where a fall occurs.

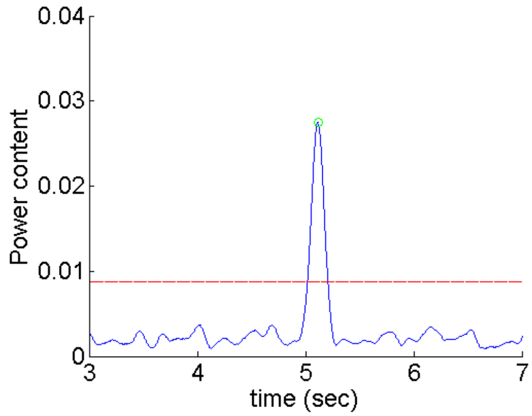

Fig. 3. An example of the PBC. The red line represents the detection threshold.

III. Feature Extraction and Classification

Once an event is detected by thresholding the PBC, we construct a 4-second window of the spectrogram, centered around each of these points that correspond to the peak frequency, to determine whether a fall has happened. The proposed technique consists of segmentation and morphological processing to obtain a clean binary time-frequency signature, and the extracted characteristics are exploited to perform sparse Bayesian classification for the determination of the type of motion represented in each window.

A. Spectrogram Segmentation and Morphological Processing

To obtain a clean binary time-frequency signature of the interested activities for the feature extraction, the following two important steps are executed on the spectrogram results: (a) image segmentation; and (b) morphological operation. In this work, the latter step includes image dilation and disconnected region removal.

The objective of image segmentation is to separate the Doppler signatures of human events from background noise. The segmentation is performed using gray-scale spectrogram images. A commonly used image segmentation technique is through proper thresholding [25], [26]. The determination of an appropriate threshold value, which separates or segments a gray-level time-frequency representation into target events and background noise regions, is an important task of a thresholding algorithm. Because the presence of the Doppler signature is usually very weak around the extreme frequencies, which are used as an important feature in the sequel, it is important that the threshold is not too high to reject such weak signals, whereas it is not too low as well so that the entire time-frequency domain is cluttered.

In addition, the spectrogram may consist of weak components, particularly around the extreme frequencies, which may yield broken segments after spectrogram segmentation [27]. Morphological operation [28], specifically dilation, can bridge closely located broken segments together. On the other hand, the removal of disconnected regions will only keep the significant time-frequency region which represents the target activities. Note that the effect of dilation should be compensated with the known number of dilated pixels when computing the peak frequencies.

Fig. 3 shows the binary time-frequency signature, corresponding to the spectrogram depicted in Fig. 2(b), respectively after segmentation and morphological operator. The threshold level used for segmentation is $\mu + 1.5\sqrt{\sigma}$, with μ and σ respectively denoting the mean and variance of the noise floor in the spectrogram, which provides a good trade-off between weak signal preservation and noise rejection. The mean and variance of the noise floor can be obtained from the spectrogram of the ambient data.

B. Feature Definition

For motion classification and fall detection, the following three features are chosen: extreme frequency magnitude, extreme frequency ratio, and length of event.

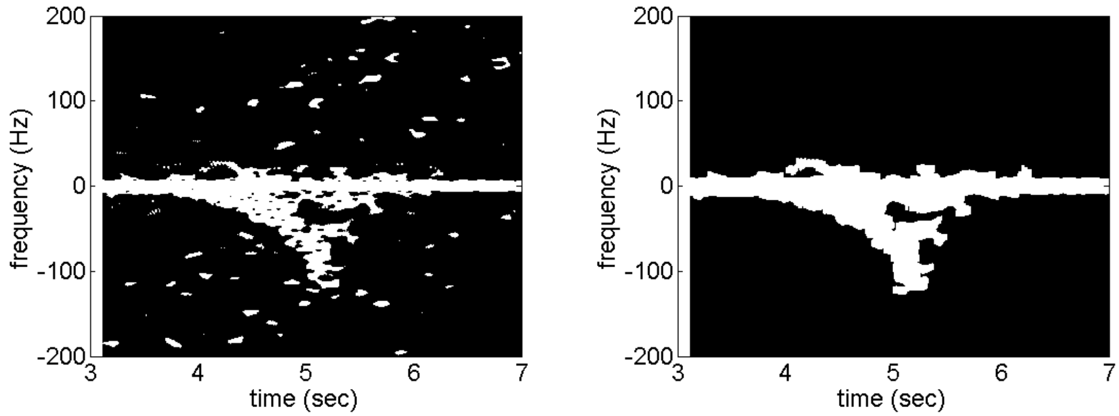

(a) after segmentation (b) after morphological operation

Fig. 4. Binary time-frequency signature obtained from the spectrogram.

1) Extreme Frequency Magnitude: The extreme frequency magnitude is defined as

$$F = \max(f_{+\max}, -f_{-\min}), \tag{9}$$

where $f_{+\max}$ and $f_{-\min}$, respectively, denote the maximum frequency in the positive frequency range and the minimum frequency in the negative frequency range. Critical falls often exhibit a high extreme frequency magnitude when compared to other types of observed motions.

2) Extreme Frequency Ratio: The extreme frequency ratio is defined as

$$R = \max\left(\left|\frac{f_{+\max}}{f_{-\min}}\right|, \left|\frac{f_{-\min}}{f_{+\max}}\right|\right). \tag{10}$$

For falls, due to the translational motion of the entire body, high energy spectrogram is concentrated in either the positive or negative frequencies, resulting in a high extreme frequency ratio. On the other hand, other types of motions, such as sitting and standing, often demonstrate high energy content in both the positive and negative frequency bands because different body parts behave with different motion patterns, thereby corresponding to a low extreme frequency ratio.

3) Length of Event: This feature describes the length of time, in milliseconds, between the start and the end of an event, i.e.,

$$L = t_{\text{extrm}} - t_{\text{begin}}, \tag{11}$$

where t_{extrm} denotes the time where the extreme frequency occurs, whereas t_{begin} denotes the corresponding beginning time the event has initiated. The beginning time of an event is determined by the time when the magnitude of the frequency content of a signal passes a specific threshold. The different motion patterns being compared in this work generally show distinct time spans.

The three features described above, i.e., the extreme frequency magnitude, the extreme frequency ratio, and the length of event, extracted from the spectrogram will be used for fall detection. The sparse Bayesian classification algorithm, which is detailed in the following section, is applied to classify fall or non-fall events. The classifier uses these features, denoted as $\mathbf{x}_n = [F_n, R_n, L_n]^T \in \mathcal{R}^3$ for the nth event, as the input, and produces t_n as the output of event such that $t_n = 1$ when the event is a fall, and $t_n = 0$ when the event is not a fall.

IV. Sparse Bayesian Classification

The three features described above, i.e., the extreme frequency magnitude, the extreme frequency ratio, and the length of event, extracted from the spectrogram will be used for fall detection. The sparse Bayesian classification algorithm, which is detailed in this section, is applied to classify fall or non-fall events. The classifier uses these features, denoted as $\mathbf{x}_n = [F_n, R_n, L_n]^T \in \mathcal{R}^3$ for the nth event, as the input, and produces t_n as the output of event with two classes. That is, t_n takes a value of 1 when the event is a fall, and its value is 0 when the event is not a fall.

Such a two-class classification is implemented by evaluating the posterior probability of an event under test, $\mathbf{x}$, belongs to each of the two classes. Such posterior probability can be generally represented in terms of the logistical sigmoid function,

$$\rho(y) = \frac{1}{1+e^{-y}}, \tag{12}$$

as [21], [22],

$$p(\mathbf{t}|\mathbf{w}) = \prod_{n=1}^{N} \rho\{y(\mathbf{x}_n, \mathbf{w})\}^{t_n}[1-\rho\{y(\mathbf{x}_n, \mathbf{w})\}]^{1-t_n}, \tag{13}$$

where $t_n \in \{0, 1\}$ is a binary variable and follows the Bernoulli distribution with the weight of $\rho\{y(\mathbf{x}_n, \mathbf{w})\}$, and $y(\mathbf{x}_n, \mathbf{w})$ is defined as the weighted summation over the base kernel $K(\mathbf{x}, \mathbf{x}_i)$ for a given set of training data $\mathbf{x}_i, i = 1, ..., N$, that is

$$y(\mathbf{x}, \mathbf{w}) = \sum_{i=1}^{N} w_i K(\mathbf{x}, \mathbf{x}_i) + w_0. \tag{14}$$

The weights $\mathbf{w} = \{w_0, w_1, \cdots, w_N\}$ will be automatically learned to enforce the sparseness and capture the most relevant vectors. The kernel function $K(\cdot)$ effectively defines a basis function for each example in the training set, and can be of the form of Gaussian, Euclidean distance, Laplacian polynomial, etc. Unlike in the SVM, the kernel in the RVM does not have to be a Mercer kernel.

We place a zero-mean Gaussian prior distribution over $\mathbf{w}$,

$$p(\mathbf{w}|\boldsymbol{\alpha}) = \prod_{i=0}^{N} \mathcal{N}(w_i|0, \alpha_i^{-1}), \tag{15}$$

where $\boldsymbol{\alpha} = [\alpha_0, ..., \alpha_N]^T$ is a vector of $N+1$ hyperparameters denoting the respective precision (reciprocal of variance). Because of the discontinuity of the likelihood in (13), neither the weight posterior $p(\mathbf{w}|\mathbf{t}, \boldsymbol{\alpha})$ nor the marginal distribution $p(\boldsymbol{\alpha}|\mathbf{t})$ can be analytically evaluated and acquired in a closed form. We thus choose to utilize the Laplace's approximation method for the estimation of the weight vector $\boldsymbol{\alpha}$. Given the hyperparameters $\boldsymbol{\alpha}$, we maximize the posterior distribution to acquire updated weight vector $\mathbf{w}$, and then $\boldsymbol{\alpha}$ is updated based on the estimated $\mathbf{w}$. As such, $\boldsymbol{\alpha}$ and $\mathbf{w}$ are obtained through an iteration procedure which is terminated when the convergence criterion is satisfied. More specifically, $\mathbf{w}_{\text{MAP}}$ can be expressed as based on the maximum a posteriori (MAP) estimation by [21],

$$\mathbf{w}_{\text{MAP}} = \boldsymbol{\Sigma}\boldsymbol{\Phi}^T\mathbf{B}\mathbf{t}, \tag{16}$$

$$\boldsymbol{\Sigma} = (\boldsymbol{\Phi}^T\mathbf{B}\boldsymbol{\Phi} + \mathbf{A})^{-1}, \tag{17}$$

$$\mathbf{A} = \text{diag}(\alpha_0, \cdots, \alpha_N), \tag{18}$$

$$\mathbf{B} = \text{diag}(\beta_1, \cdots, \beta_N), \tag{19}$$

$$\beta_n = \rho\{y(\mathbf{x}_n, \mathbf{w})\}[1 - \rho\{y(\mathbf{x}_n, \mathbf{w})\}], \tag{20}$$

where $\boldsymbol{\Phi} = [\boldsymbol{\phi}(\mathbf{x}_1), \boldsymbol{\phi}(\mathbf{x}_2), \cdots, \boldsymbol{\phi}(\mathbf{x}_N)]^T$ and $\boldsymbol{\phi}(\mathbf{x}_n) = [1, K(\mathbf{x}_n, \mathbf{x}_1), K(\mathbf{x}_n, \mathbf{x}_2), \cdots, K(\mathbf{x}_n, \mathbf{x}_N)]^T$. Given a specific $\boldsymbol{\alpha}$, the $\mathbf{w}_{\text{MAP}}$ is updated in Eq. (16), the associated learning problem becomes a search for the hyperparameter $\boldsymbol{\alpha}$. We define a new variable $\hat{\mathbf{t}}$ as

$$\hat{\mathbf{t}} = \boldsymbol{\Phi}\mathbf{w}_{\text{MAP}} + \mathbf{B}^{-1}(\mathbf{t} - \mathbf{y}). \tag{21}$$

A type-II maximum likelihood approximation employs a point estimate for $\boldsymbol{\alpha}$ to maximize the approximate log marginal likelihood [21], [29], [30], [31], [32],

$$L(\boldsymbol{\alpha}) = -\frac{1}{2}\left[N \log 2\pi + \log|\mathbf{C}| + \hat{\mathbf{t}}^T \mathbf{C}^{-1}\hat{\mathbf{t}}\right], \tag{22}$$

where $\mathbf{C} = \mathbf{B} + \boldsymbol{\Phi}\mathbf{A}\boldsymbol{\Phi}^T$. We acquire the updated expression of α_n based on the fast greedy algorithms [22], [32],

$$\alpha_n = \begin{cases} \dfrac{s_n^2}{q_n^2 - s_n}, & \text{if } q_n^2 > s_n, \\ \infty, & \text{if } q_n^2 \leq s_n, \end{cases} \tag{23}$$

where $s_n = \boldsymbol{\phi}^T(\mathbf{x}_n)(\mathbf{C}_{-n})^{-1}\boldsymbol{\phi}(\mathbf{x}_n)$, $q_n = \boldsymbol{\phi}^T(\mathbf{x}_n)(\mathbf{C}_{-n})^{-1}\hat{\mathbf{t}}$ and $\mathbf{C}_{-n} = \mathbf{C} - \alpha_n^{-1}\boldsymbol{\phi}(\mathbf{x}_n)\boldsymbol{\phi}^T(\mathbf{x}_n)$. Note that Eq. (23) shows the *pruned-out* operator. That is, when $q_n^2 > s_n$, α_n adopts a nonzero value and the corresponding atom would be kept as a relevance vector. On the other hand, when $q_n^2 \leq s_n$, the atom would be pruned out from the model. It is observed that the sparse Bayesian learning based on RVM strongly encourages the sparseness of the weight vector compared with the SVM and thus acquires much fewer relevance vectors in the resulting model.

V. Experiment Results

A. *Experiment Settings*

We conducted experiments for 8 different motion patterns, with each experiment pattern repeated for 10 times (5 times each for 2 objects). The recording time for each experiment is 20 seconds. Every set of experiments contains a different type of motion, including forward falling, backward falling, sitting and standing, and bending over and standing up. We also split each motion pattern into two different variations, one demonstrating a standard type of motion whereas the other one demonstrating a high-energy form of that motion in order to study the impact of such variations on the classification performance. The typical spectrograms of the 8 motion patterns are shown in Fig. 5. The first 4 patterns are collectively considered as falls, whereas the last 4 patterns are collectively considered as non-falls. Our objective is to correctly detect fall events from non-fall events.

B. Feature Extraction and Classification Results

Fig. 6 shows the ground truth of three features defined in Section III, i.e., the extreme frequency magnitude, the extreme frequency ratio, and the length of event. Specifically, Fig. 6(a) shows the three-dimensional (3-D) view of the three features, whereas their pairwise two-dimensional (2-D) plots are respectively shown in Figs. 6(b)–6(d). It is observed that these features generally provide a clear distinction between the fall and non-fall events, except one outlier fall event (marked with a circle). Examination of the spectrogram of this outlier fall event shows that the signal is very weak, yielding low extreme Doppler frequency as well as a short length of event time.

The fall events exhibit larger extreme frequency magnitudes, higher extreme frequency ratios, and longer lengths of event time than the non-fall counterparts. These features, however, does not robustly classify the fall and non-fall activities based on a singe feature alone.

The sparse Bayesian classification algorithm and the SVM algorithm are respectively applied by using a Gaussian kernel, which is defined as $K(\mathbf{x}_m, \mathbf{x}_n) = \exp(-\|\mathbf{x}_m - \mathbf{x}_n\|^2/r^2)$ with the width parameter chosen as $r = 0.5$. We use 5-fold cross-validation on the motion data. The entire sample set is randomly partitioned into 5 equal-size subsets. Out of the 5 subsets, a single subset is retained as the validation data for testing the classifier, and the remaining 4 subsets are used as the training data. The cross-validation process is repeated 5 times, with each of the 5 subsets used exactly once as the validation data.

Both algorithms acquire similar results with one misclassification of the outlier fall event as described earlier, as shown Fig. 7(a), where the misclassified result is marked in circle. The number of relevance vectors required in the sparse Bayesian classification are around 5, which is much smaller when compared with the 20 support vectors obtained in the SVM. It is found that the number of support vectors required generally grows linearly with the size of training data in the experiments. Although the number of samples is limited in the current experimental study, the classification method based on the RVM technique acquires the same accuracy with far less relevance vectors. In practical applications, the number of data samples will be large and, thereby, the advantages of RVM will be more pronounced. Furthermore, the sparse Bayesian classification algorithm also acquires the probability of fall motion so that we can evaluate uncertainty in the prediction, as shown Fig. 7(b). In this figure, the index of experiment is ordered with forward falling, forward falling with arm motion, backward falling, backward falling with arm motion, sitting and standing, fast sitting and standing, bending over and standing up, and fast bending over and standing up (refer to Fig. 5), each of 10 trials. We observe in Fig. 7(b) that the fall events generally show a high probability of fall motion except the outlier event. For non-fall events, the normal sit-and-stand and bend-and-stand-up activities show consistent low probability of fall motion, whereas the fast sit-and-stand and bend-and-stand-up activities tend to exhibit a higher probability of fall motion, although their absolute value remains low for reliable classification.

VI. Conclusion

We have proposed an effective technique to process radar Doppler signatures for fall detection. The proposed technique treats the spectrogram as a gray-scale image, and image segmentation and morphological processing of spectrogram are performed before it is passed to perform feature analysis. Three features, namely, the extreme frequency magnitude, extreme frequency ratio, and the length of event, are extracted from the processed spectrogram, and the results are used to perform sparse Bayesian classification for proper fall detection. Experiment results validated the effectiveness of the proposed technique.

ACKNOWLEDGEMENT

The authors are grateful to Dr. Fauzia Ahmad, Director of the Radar Imaging Lab, Villanova University, for her kind help in performing the data collection. They also acknowledge E. Ulmer and L. Ramirez Rivera for their participation in the experiments and initial data processing.

REFERENCES

[1] A. Gadde, M. G. Amin, Y. D. Zhang, and F. Ahmad, "Fall detection and classifications based on time-scale radar signal characteristics," in *Proc. SPIE 9077, Radar Sensor Technology XVIII,* Baltimore, MD, May 2014.

[2] L. Ramirez Rivera, E. Ulmer, Y. D. Yimin, W. Tao, and M. G. Amin, "Radar-based fall detection exploiting time-frequency features," in *Proc. IEEE China Summit and Int. Conf. on Signal and Info. Proc.,* Xi'an, China, July 2014.

[3] *World population prospects : The 2010 Revision.* United Nations, Department of Economic and Social Affairs, Population Division, 2011. Available at http://esa.un.org/wpp/.

[4] S. Sadigh, A. Reimers, R. Andersson, and L. Laflamme, "Falls and fall related injuries among the elderly: a survey of residential-care facilities in a swedish municipality," *J. Community Health*, vol. 29, pp. 129–140, 2004.

[5] S. L. Murhy, "National vital statistics reports," tech. rep., National Center for Health Statistics, 2000.

[6] C. G. Moran, R. T. Wenn, M. Sikand, and A. M. Taylor, "Early mortality after hip fracture: is delay before surgery important," *J. Bone and Joint Surgery*, vol. 87, pp. 483–489, 2005.

[7] M. Chuah and F. Fu, "ECG anomaly detection via time series analysis," in *Proc. Int. Symp. Parallel and Distributed Proc. and Appli.*, pp. 121–140, Niagara Falls, Canada, Aug. 2007.

[8] A. Høst-Madsen, N. Petrochilos, O. Boric-Lubecke, V. M. Lubecke, B.-K. Park, and Q. Zhou, "Signal processing methods for Doppler radar heart rate monitoring," in D. Mandic, M. Golz, A. Kuh, D. Obradovic, and T. Tanaka (Eds.), *Signal Processing Techniques for Knowledge Extraction and Information Fusion,* Springer, pp. 121–140, 2008.

[9] O. Aardal, S.-E. Hamran, T. Berger, J. Hammerstad, and T. S. Lande, "Radar cross section of the human heartbeat and respiration in the 500mhz to 3ghz band," in *Proc. IEEE Radio and Wireless Symp.*, pp. 422–425, Phoenix, AZ, Jan. 2011.

[10] M. G. A. (Ed.), *Through the Wall Radar Imaging*. CRC Press, 2011.

[11] Y. Zhang, M. G. Amin, and F. Ahmad, "A novel approach for moving multi-target localization using dual frequency radars and time-frequency distributions," in *Proceedings of Annual Asilomar Conference on Signals, Systems, and Computers,* Pacific Grove, CA, Nov. 2007.

[12] B. Mobasseri and M. G. Amin, "A time-frequency classifier for human gait recognition," in *Proc. SPIE,* vol. 7306, 2009.

[13] F. C. Tivive, A. Bouzerdoum, and M. G. Amin, "A human gait classificationmethod based on radar Doppler spectrograms," *EURASIP J. Adv. Sig. Proc.*, vol. 2010, pp. 1–12, 2010.

[14] Y. Kim and H. Ling, "Human activity classification based on micro-Doppler signatures using a support vector machine," *IEEE Trans. Geoscience and Remote Sensing*, vol. 47, pp. 1328–1337, 2009.

[15] L. Liang, M. Popescu, M. Skubic, M. Rantz, T. Yardibi, and P. Cuddihy, "Automatic fall detection based on doppler radar motion signature," in *Proceedings of the 5th International Conference on Pervasive Computing Technologies for Healthcare (PervasiveHealth)*, pp. 222–225, 2011.

[16] P. Karsmakers, T. Croonenborghs, M. Mercuri, D. Schreurs, and P. Leroux, "Automatic in-door fall detection based on microwave radar measurements," in *Proceedings of the 9th European Radar Conference*, pp. 202–205, 2012.

[17] B. Boser, I. Guyon, and V. N. Vapnik, "A training algorithm for optimal margin classifiers," in *Proc. of the Fifth Annual Workshop on Computational Learning Theory*, pp. 144–152, 1992.

[18] C. J. C. Burges, "Simplified support vector decision rules," in *Proc. of the Thirteenth International Conference on Machine Learning*, pp. 71–77, 1996.

[19] P. Vincent and Y. Bengio, "Kernel matching pursuit," *Machine Learning*, vol. 48, pp. 165–187, 2002.

[20] S. S. Keerthi, O. Chapelle, and D. DeCoste, "Building support vector machines with reduced classifier complexity," *Journal of Machine Learning Research*, vol. 7, pp. 1493–1515, 2006.

[21] M. E. Tipping, "Sparse Bayesian learning and the relevance vector machine," *Journal of Machine Learning Research*, vol. 1, no. 9, pp. 211–244, 2001.

[22] C. M. Bishop, *Pattern Recognition and Machine Learning*. Springer, 2006.

[23] L. Liu, M. Popescu, M. Skubic, M. Rantz, T. Yardibi, and P. Cuddihy, "Automatic fall detection based on Doppler radar motion signature," in *Proc. IEEE Int. Conf. Pervasive Computing Tech. for Healthcare*, pp. 222–225, 2011.

[24] M. Wu, X. Dai, Y. D. Zhang, B. Davidson, J. Zhang, and M. G. Amin, "Fall detection based on sequential modeling of radar signal time-frequency features," in *Proc. IEEE Int. Conf. Healthcare Informatics,* Philadelphia, PA, Sept. 2013.

[25] W. Tao, H. Jin, Y. Zhang, L. Liu, and D. Wang, "Image thresholding using graph cuts," *IEEE Trans. Systems, Man and Cybernetics, Part A*, vol. 38, pp. 1181–1195, Sep. 2008.

[26] W. Tao, H. Jin, and Y. Zhang, "Color image segmentation based on mean shift and graph cuts," *IEEE Trans. Systems, Man and Cybernetics, Part B*, vol. 37, pp. 1382–1389, Oct. 2007.

[27] P. Heidenreich, L. Cirillo, and A. Zoubir, "Morphological image processing for fm source detection and localization," *Signal Proc.*, vol. 89, pp. 1070–1080, 2009.

[28] R. Gonzalez and R. Woods, *Digital Image Processing*. Oxford, 2001.

[29] Q. Wu, Y. D. Zhang, M. G. Amin, and B. Himed, "Complex multitask Bayesian compressive sensing," in *Proc. IEEE ICASSP*, Florence, Italy, May 2014.

[30] S. Ji, Y. Xue, and L. Carin, "Bayesian compressive sensing," vol. 56, no. 6, pp. 2346–2356, 2008.

[31] Z. Zhang and B. D. Rao, "Extension of SBL algorithm for the recovery of block sparse signals with inter-block correlation," vol. 92, no. 7, pp. 1580–1590, 2012.

[32] M. E. Tipping, "Fast marginal likelihood maximization for sparse Bayesian models," in *Proc. of the Ninth International Workshop on Artificial Intelligence and Statistics*, 2003.

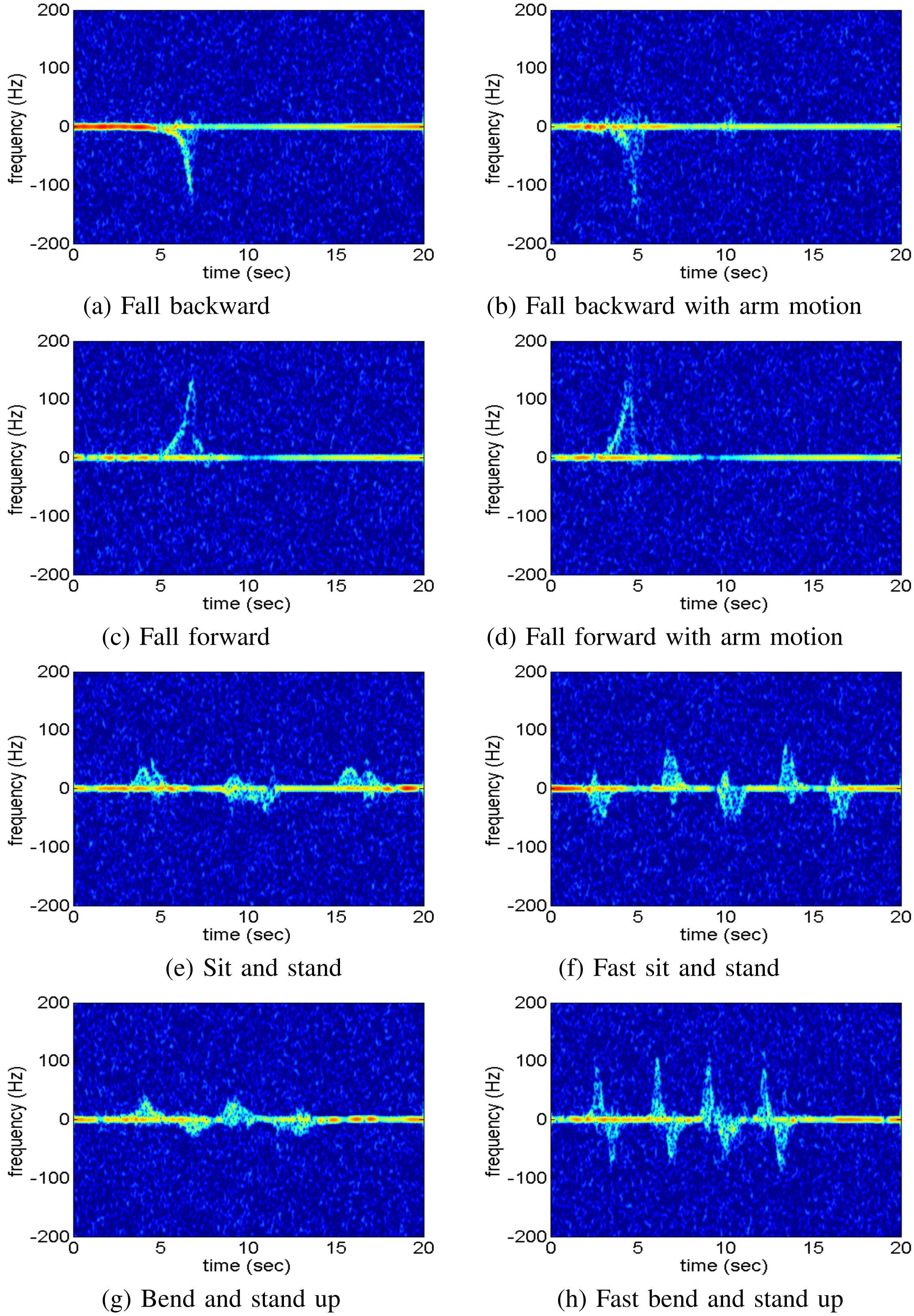

(a) Fall backward

(b) Fall backward with arm motion

(c) Fall forward

(d) Fall forward with arm motion

(e) Sit and stand

(f) Fast sit and stand

(g) Bend and stand up

(h) Fast bend and stand up

Fig. 5. Spectrogram of typical motion patterns.

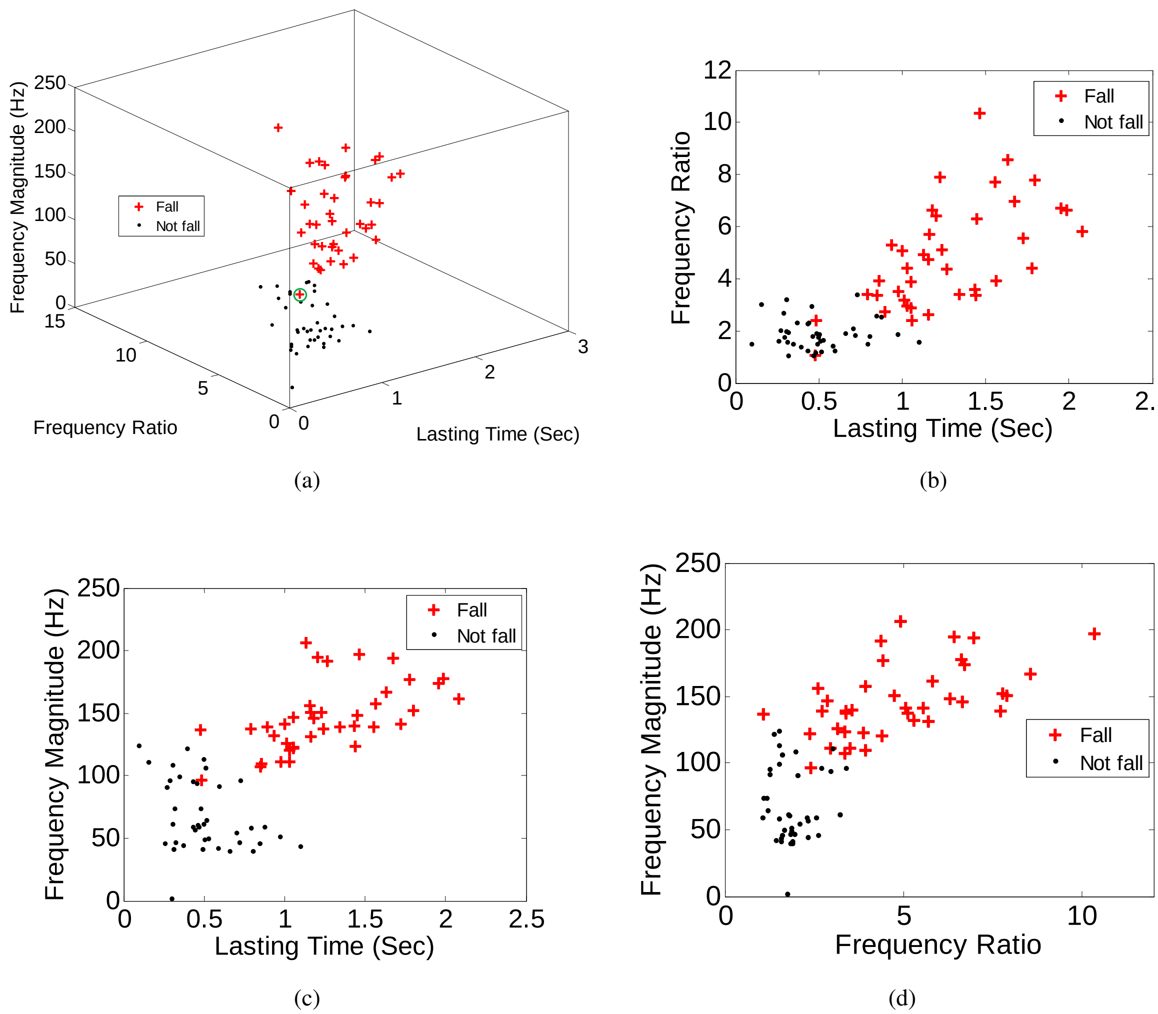

Fig. 6. Ground truth of motions with 3-D vision and three 2-D visions.

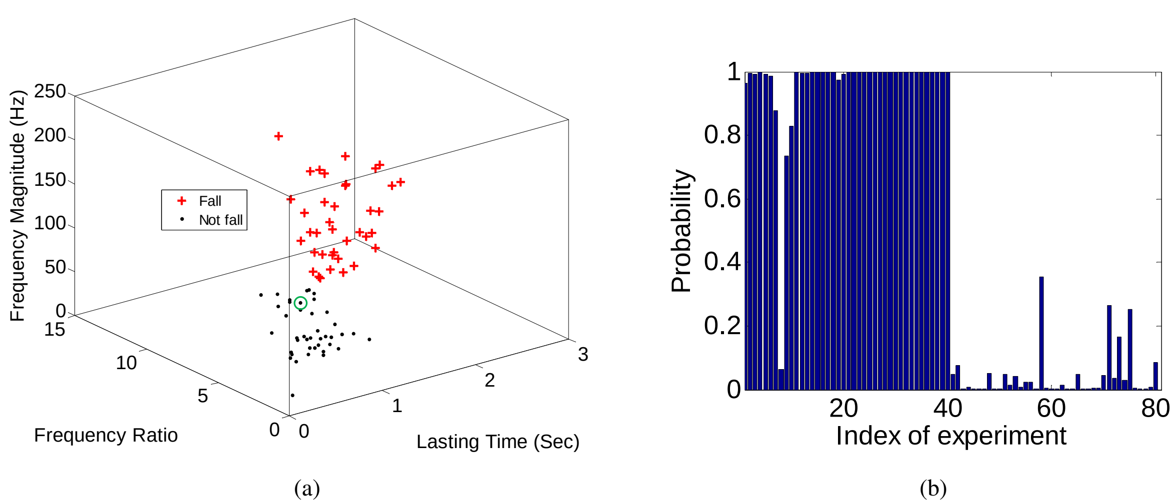

Fig. 7. (a) Classification result based on sparse Bayesian algorithm. (b) Probability distribution of fall motion.